Ion Formation from Alkali Halide Solids by High Power Pulsed Laser Irradiation *

B. Jöst, B. Schueler, and F. R. Krueger

Institut für Biophysik, Physik für Mediziner, Frankfurt (Main)

Ion formation from alkali halide solids caused by the irradiation of high power (some 10^8 W/cm^2) pulsed lasers is investigated by means of time-of-flight mass spectrometry (LAMMA®). It is shown that the ions are formed directly from the solid state, several uppermost atomic layers being involved; gas phase interactions are negligible. The ion formation rates, however, are incompatible with the assumption of a quasiequilibrium phase transition, but should be explained in terms of non-adiabatic rate processes discussed in some detail. The light absorption of the transparent halide crystals is assumed to be initiated by multiphoton absorption — free electron production; the further energy transfer being maintained by rapid polaron-Joule-heating. The data are compatible with this model.
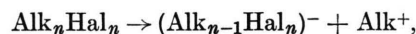
1. Introduction

In the past various studies of ion production from solid materials, e.g. metals [1], covalently bound systems [2], polar organic compounds [3], and alkali halides [4] under laser irradiation were performed. It was found that each class of substances yields specific ion types in the mass spectra from the LAMMA®-instruments [13]. For homonuclear systems (like carbon or metals) a vaporization model was presented by Fürstenau [5].

However, there is great demand for a better understanding of ion production from polar and ionic compounds. Typical ions occuring in the mass spectra of polar organic molecules M are e.g. the protonated $(M+H)^+$ and the deprotonated $(M-H)^-$ quasimolecular ions, resulting from reactions of the type

$$n\,M \rightarrow ((n-1)\,M - H)^- + (M+H)^+,$$
$$n\,M \rightarrow ((n-1)\,M + H)^+ + (M-H)^-.$$
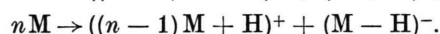
This is similar to ion types obtained from alkali halides,

$$Alk_n Hal_n \rightarrow (Alk_{n-1} Hal_n)^- + Alk^+,$$
$$Alk_n Hal_n \rightarrow (Alk_n Hal_{n-1})^+ + Hal^-.$$

One may be able to describe relative cation yields by the proton affinities of polar organic molecules or alkali affinities for alkali halides, respectively. However, alkali halides represent a simple limiting case of ionic systems and should consequently lead more easily to a better insight to the ion production process from polar organic molecules.

For a complete description of the ion generation process one must be able to separate the energy transfer process from the laser beam into the lattice from the ion formation process itself. It will be shown that the ion formation threshold irradiance is mainly determined by the primary excitation process, whereas the distribution of the relative ion intensities can be described by parameters of the solid crystals. Difficulties arise from the impossibility of a complete separation of these two processes because their interdependance is not yet known. In this paper the experimental data are parametrized according to the model presented.

2. The Initiation Process of Laser Energy Absorption in Alkali Halides

It is assumed that the ion formation is initiated in four steps (Fig. 1), namely irradiation of the transparent crystal, population of the conduction band (cb), excitation of the cb-electrons, and energy transfer to the lattice.

Especially for alkali halides the production of cb-electrons is expected to be mainly due to multiphoton processes. From this point of view the critical parameter is the ratio of the band gap and the photon energy, determining the order N of the multiphoton excitation process. This hypothesis
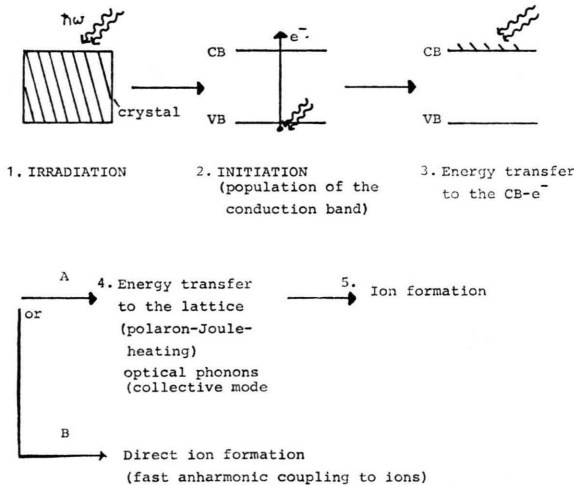
Fig. 1. Schematic diagram of the initiation process of ion formation from dielectric solids.

includes that a sufficient cb-electron concentration must be produced, which is able to absorb energy from the laser beam via polaron (individual or collective electron-phonon-interaction) Joule heating, as introduced by Bräunlich et al. [6]. If enough energy is offered to the solid a breakdown can be initiated; in this case the formation of free ions takes place.

The assumption that the ion detection threshold is mainly determined by the primary excitation process has been investigated experimentally. The ion detection threshold is defined to be the laser irradiance leading to a 50% probability of ion detection. The threshold irradiance is expected to vary in accordance with the order N of the multi-

photon excitation process. If N is kept constant, no essential threshold variations thus should occur.

In the experiments the ion detection threshold was measured for small Cs- and Rb- halide crystals prepared by air drying from aquous solutions, this simple technique yielding reproducible results. The relative threshold ratios of all these substances were determined for each laser wave length separately because the relative threshold values at constant wavelength for various substances can be determined more confidently than with various wavelenghts at one substance. Therefore various N ($N = \mathrm{Int}(E_{\mathrm{gap}}/\hbar\omega_{\mathrm{laser}}) + 1$) were realized by variation of the band gap energy E_{gap} alone. This was made for various frequencies ω_{laser}.

A Q-switched ($t_{\mathrm{p}} = 10$ nsec) Nd-Yag laser operating in the TEM OO mode was used. The experiments were performed at the wave lengths 266 nm, 355 nm, and 532 nm [13]. Every laser shot was energy monitored by means of a photodiode detector.

The experimental results of the threshold values are listed in Table 1. The data are in agreement with the hypothesis that the threshold energy increases with increasing order of the multiphoton process in question. The band gap data used were taken from [7].

Under the assumption that the main contribution to the threshold irradiance results from the carrier generation process to yield a determined carrier density $n_{\mathrm{cb}}(t)$ within the laser pulse length t_{p}, the threshold irradiance can be estimated. The photon fluxes which are necessary to create carrier concentrations between $10^{19} - 10^{22}$ cm^{-3} have been

Table 1. Threshold ratios for Cesium- and Rubidium halides obtained experimentally (e) for $\lambda = 266$ nm, 355 nm, and 532 nm, and calculated ratios (c) from Eq. (1) using $n_{\mathrm{cb}}(t_{\mathrm{p}}) = 10^{22}$ cm^{-3} under the assumption that the same carrier density is produced for all substances. N(AlkHal) indicates the minimum order necessary for the multiphoton initiation process. A is the peak flux density.

	266 nm	355 nm	532 nm		355 nm	532 nm
N(CsF)	3	3	5	N(RbF)	3	5
$\dfrac{A_{\mathrm{th}}(\mathrm{CsF})}{A_{\mathrm{th}}(\mathrm{CsCl})}$	3 (e) 13 (c)	1 (e) 1 (c)	1.2 (e) 1.4 (c)	$\dfrac{A_{\mathrm{th}}(\mathrm{RbF})}{A_{\mathrm{th}}(\mathrm{RbCl})}$	1.1 (e) 1 (c)	1.3 (e) 1.4 (c)
N(CsCl)	2	3	4	N(RbCl)	3	4
$\dfrac{A_{\mathrm{th}}(\mathrm{CsCl})}{A_{\mathrm{th}}(\mathrm{CsBr})}$	1 (e) 1 (c)	1 (e) 1 (c)	1.6 (e) 1.7 (c)	$\dfrac{A_{\mathrm{th}}(\mathrm{RbCl})}{A_{\mathrm{th}}(\mathrm{RbBr})}$	1 (e) 1 (c)	1 (e) 1 (c)
N(CsBr)	2	3	3	N(RbBr)	3	4
$\dfrac{A_{\mathrm{th}}(\mathrm{CsBr})}{A_{\mathrm{th}}(\mathrm{CsJ})}$	1.1 (e) 1 (c)	3.2 (e) 13 (c)	1 (e) 1 (c)	$\dfrac{A_{\mathrm{th}}(\mathrm{RbBr})}{A_{\mathrm{th}}(\mathrm{RbJ})}$	2.8 (e) 13 (c)	1.5 (e) 1.7 (c)
N(CsJ)	2	2	3	N(RbJ)	2	3

calculated for $N = 2, 3, 4, 5$ from [6]

$$n_{cb}(t_p) = n_{vb}(t = 0)$$
$$\cdot \left\{ 1 - \exp\left(- \int_0^{t_p} \sigma^{(N)} F^N(t') \, dt' \right) \right\},$$

$\sigma^{(N)}$ being the N-photon cross section, $n_{cb}(t_p)$ the carrier concentration at the end of the laser pulse, t_p the laser pulse length, $n_{vb}(0)$ the initial density of valence electrons and $F(t)$ the photon flux, which was taken as $F(t) = A \sin^2(\pi t/t_p)$, where A is the peak photon flux density.

However, the calculation of the flux density necessary to create fixed carrier densities within the same time for all substances provides qualitative trends for the threshold ratios for different multiphoton order N. The calculated and the experimental threshold ratios are shown in Table 1. The calculated ratios of the photon flux density $A(N+1)/A(N)$ decrease with increasing order N of the multiphoton process. This is also represented by the experimental threshold ratios. The experimental threshold irradiances were about 10^9 W/cm², and the irradiance to create a sufficient carrier density of about 10^{19} cm⁻³ for $\lambda = 355$ nm for CsF is in this order of magnitude, too. Therefore the ion detection threshold seems to be mainly determined by the initiation process.

It should be pointed out that no quantitative agreement between the measured and the calculated threshold values can be expected, for example because of the undefined surface properties of the alkali halide samples. However, the relative order of thresholds is expected to be realized with uniform preparational conditions.

3. Ion Formation from Condensed Media

Before discussing and parametrizing the ion formation from alkali halides a brief overview of the models is given which could be reasonably applied for the ion generation methods described in this paper. An operational hierarchy of the models of ion formation is given in Figure 2.

The method of rate processes [8] starts from the description of the time behaviour of a closed system (by the von Neumann equation) consisting of the subsystem in question (i.e. any molecular state of an alkali halide atomic or cluster ion) and the surrounding medium (the alkali halide lattice). If the mean relaxation time of the vibrational states in

A
Adiabatic Rate Processes
model: transitions between two stable or quasistable nuclear configurations of the *same* electronic potential curves, the electronic and the molecular system is relaxed within the whole transition

↓

B
Diabatic Rate Processes
model: transitions between two different intersecting electronic potential curves, the nuclear system can be relaxed *within* the two potential curves. The transition is a fast change of the potential energy without relaxation along the reaction coordinate

Extreme B₁
approximation: slow transition, fast excitation and relaxation, detailed balance

Extreme B₂
approximation: fast transition, slow excitation and relaxation, detailed balance

Extreme diabatic D
non-Markovian process, no detailed balance, fast oszillatoric change of the electronic potential, quantum mechanical treatment
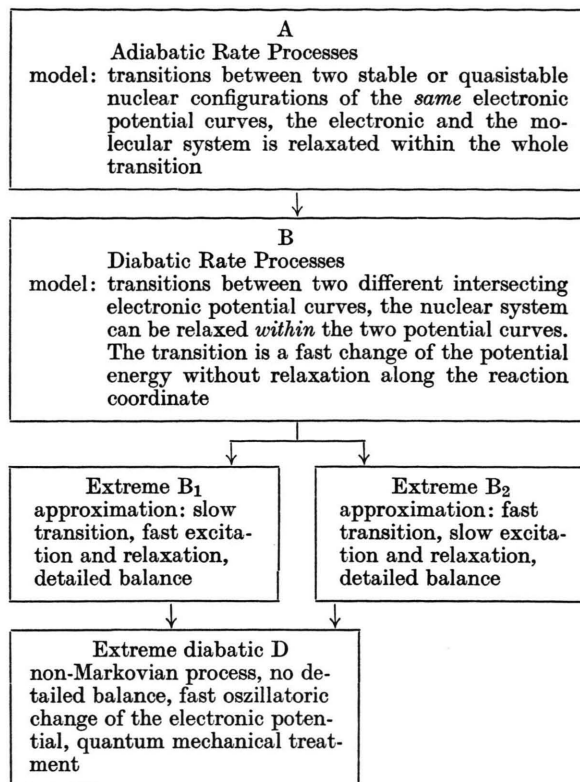
Fig. 2. Hierarchy of ion formation models.

the condensed medium is much smaller than that of the states of the considered subsystem responsible for ion formation (surface states, activated complex states, free states) it is possible to derive the time behaviour of that subsystem (represented by its density matrix) from the von Neumann equation for the density matrix of the whole system, thus fulfilling the condition for the application of a Markov approximation. If this subsystem has non-degenerate energy levels one may approximate the set of conditional occupation probabilities of the levels of this very subsystem by a master equation.

Assuming the master equation description to be applicable we first discuss adiabatic rate processes. The principal situation is shown in Figure 3. In this case the transition is described by the overcoming of a potential barrier from a stable configuration of the bound molecular system to a free state. It is essential that in this case the transition takes place on the same electronic potential curve. This means that during the whole reaction the molecular system thus forming the electronic charge
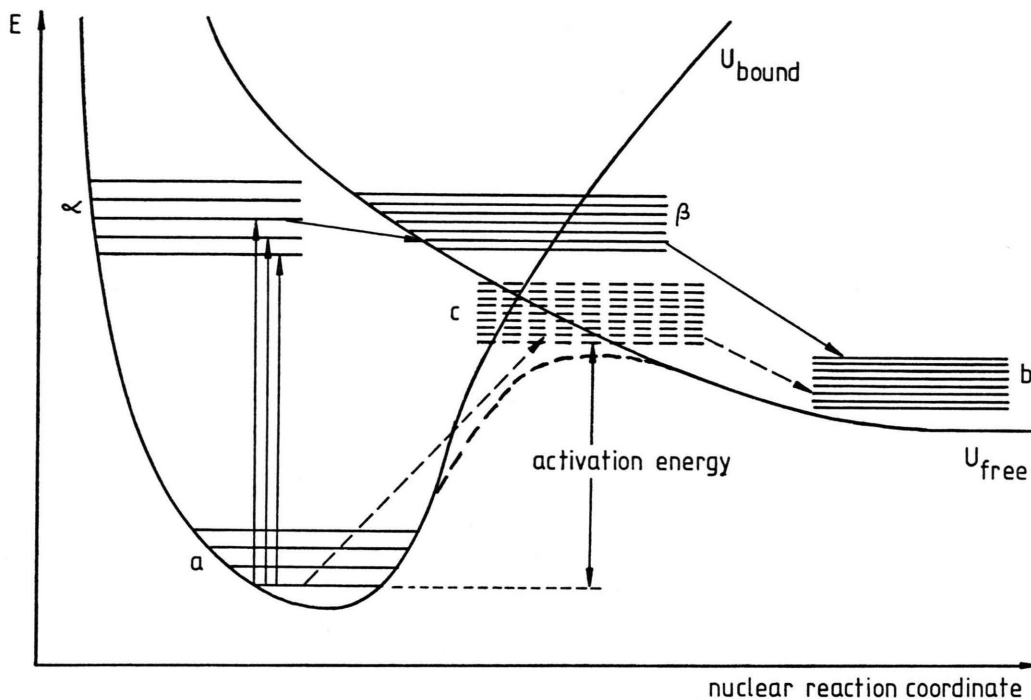
Fig. 3. Two different intersecting energy hypersurfaces (solid lines) of the bound (lattice) and the free atomic system (gas phase) forming the ion. The broken line indicates its electronic adiabatic potential.

distribution (for closed-shell atoms) is relaxed at any point along the reaction coordinate (distance of the center of mass to the surface plane). Thus the "adiabatic transition" is described by a chain of subsequent equilibrium steps. The master equations for the adiabatic rate process are [9]:

$$\dot{P}_{\mathrm{a}} = -\sum_{\mathrm{a}'}(w_{\mathrm{aa}'}P_{\mathrm{a}} - w_{\mathrm{a}'\mathrm{a}}P_{\mathrm{a}'})$$
$$+ \sum_{\mathrm{c}}(w_{\mathrm{ca}}P_{\mathrm{c}} - w_{\mathrm{ac}}P_{\mathrm{a}})$$
$$\dot{P}_{\mathrm{b}} = -\sum_{\mathrm{b}'}(w_{\mathrm{bb}'}P_{\mathrm{b}} - w_{\mathrm{b}'\mathrm{b}}P_{\mathrm{b}'})$$
$$+ \sum_{\mathrm{c}}(w_{\mathrm{cb}}P_{\mathrm{b}} - w_{\mathrm{bc}}P_{\mathrm{c}})$$
$$\dot{P}_{\mathrm{c}} = \sum_{\mathrm{a}}(w_{\mathrm{ac}}P_{\mathrm{a}} - w_{\mathrm{ca}}P_{\mathrm{c}})$$
$$+ \sum_{\mathrm{b}}(w_{\mathrm{bc}}P_{\mathrm{b}} - w_{\mathrm{cb}}P_{\mathrm{c}})$$
$$- \sum_{\mathrm{c}'}(w_{\mathrm{cc}'}P_{\mathrm{c}} - w_{\mathrm{c}'\mathrm{c}}P_{\mathrm{c}'}),$$

where the w_{xy} are the transition probabilities per unit time from a state E_x to a state E_y if E_x is populated and the P_i are the population probabilities of the states E_{a}, E_{b} and E_{c}.

If the relaxation between the microstates c of the activated complex is much faster than transi-

tions between c and microstates a or b the rate constant k_{AB} can be written as

$$k_{\mathrm{AB}} = \gamma_{\mathrm{CA}}\gamma_{\mathrm{CB}}(\gamma_{\mathrm{CA}} + \gamma_{\mathrm{CB}})^{-1}$$
$$\cdot \exp(-(F_{\mathrm{C}} - F_{\mathrm{A}})/kT)$$

with

$$\gamma_{\mathrm{CA}} = \sum_{\mathrm{c}} w_{\mathrm{ca}}\exp(-E_{\mathrm{c}}/kT)/\sum_{\mathrm{c}}\exp(-E_{\mathrm{c}}/kT),$$
$$\gamma_{\mathrm{CB}} = \sum_{\mathrm{c}} w_{\mathrm{cb}}\exp(-E_{\mathrm{c}}/kT)/\sum_{\mathrm{c}}\exp(-E_{\mathrm{c}}/kT),$$
$$F_{\mathrm{C}} = -kT\ln\left(\sum_{\mathrm{c}}\exp(-E_{\mathrm{c}}/kT)\right),$$
$$F_{\mathrm{A}} = -kT\ln\left(\sum_{\mathrm{a}}\exp(-E_{\mathrm{a}}/kT)\right).$$

The quantity $(F_{\mathrm{C}} - F_{\mathrm{A}})$ is known as "activation energy". The rate function k_{BA}, describing a recapture of free ions by the crystal is assumed to be negligible compared with k_{AB}.

For the diabatic case corresponding to Figure 2. Block 2 shown in Fig. 3b the situation is different. The diabatic description may be applied if a perturbation acts mainly on the electronic system in such a way that the nuclear system remains non-relaxed in the changed electronic potential, e.g. formed by a rapid perturbation of the surrounding lattice. In this case the transition can be described between

two different electronic states, namely that corresponding to the charge distribution within the unperturbed lattice and that of the free gaseous state, and is thus far from equilibrium.

The master equation of a diabatic transition has the form [9]:

$$\dot{P}_{\mathrm{a}} = -\sum_{\mathrm{a}'}(w_{\mathrm{aa}'}P_{\mathrm{a}} - w_{\mathrm{a}'\mathrm{a}}P_{\mathrm{a}'})$$
$$-\sum_{\alpha}(w_{\mathrm{a}\alpha}P_{\mathrm{a}} - w_{\alpha\mathrm{a}}P_{\alpha}),$$

$$\dot{P}_{\mathrm{b}} = -\sum_{\mathrm{b}'}(w_{\mathrm{bb}'}P_{\mathrm{b}} - w_{\mathrm{b}'\mathrm{b}}P_{\mathrm{b}'})$$
$$-\sum_{\beta}(w_{\mathrm{b}\beta}P_{\mathrm{b}} - w_{\beta\mathrm{b}}P_{\beta}),$$

$$\dot{P}_{\alpha} = -\sum_{\mathrm{a}}(w_{\alpha\mathrm{a}}P_{\alpha} - w_{\mathrm{a}\alpha}P_{\mathrm{a}})$$
$$-\sum_{\beta}(w_{\alpha\beta}P_{\alpha} - w_{\beta\alpha}P_{\beta})$$
$$-\sum_{\alpha'}(w_{\alpha\alpha'}P_{\alpha} - w_{\alpha'\alpha}P_{\alpha'}),$$

$$\dot{P}_{\beta} = -\sum_{\beta}(w_{\beta\mathrm{b}}P_{\beta} - w_{\mathrm{b}\beta}P_{\mathrm{b}})$$
$$-\sum_{\alpha}(w_{\beta\mathrm{a}}P_{\beta} - w_{\alpha\beta}P_{\alpha})$$
$$-\sum_{\beta'}(w_{\beta\beta'}P_{\beta} - w_{\beta'\beta}P_{\beta'}).$$

When detailed balance within the microstates is provided one may distinguish two limiting cases for the diabatic transition.

B1 Slow excitation and relaxation within the two intersecting electronic potential curves for bound and free states, respectively, in comparison to the transition speed between states belonging to the two different electronic potentials.

In this approximation the rate function can be written as follows:

$$k_{\mathrm{AB}} = \gamma_{\mathrm{A}}\gamma_{\mathrm{B}}(\gamma_{\mathrm{A}} + \gamma_{\mathrm{B}})^{-1}$$
$$\cdot \exp(-(F_0 - F_{\mathrm{A}})/kT)$$

with

$$F_0 = -kT\ln\left(\sum_{\alpha}\exp(-E_{\alpha}/kT) + \sum_{\beta}\exp(-E_{\beta}/kT)\right),$$

$$\gamma_{\mathrm{A}} = \sum_{\alpha\mathrm{a}}w_{\alpha\mathrm{a}}\exp(-E_{\alpha}/kT)/\Sigma_0,$$

$$\gamma_{\mathrm{B}} = \sum_{\beta\mathrm{b}}w_{\beta\mathrm{b}}\exp(-E_{\beta}/kT)/\Sigma_0,$$

$$\Sigma_0 = \sum_{\alpha}\exp(-E_{\alpha}/kT) + \sum_{\beta}\exp(-E_{\beta}/kT).$$

B2 Fast excitation and relaxation within the two intersecting potentials and slow transition between the two different electronic states.

In this case the rate function takes the form:

$$k_{\mathrm{AB}} = \left(\sum_{\alpha\beta}w_{\alpha\beta}\exp(-E_{\alpha}/kT)\Big/\sum_{\alpha}\exp(-E_{\alpha}/kT)\right)$$
$$\cdot \exp(-(\tilde{F}_{\mathrm{A}} - F_{\mathrm{A}})/kT)$$

with

$$\tilde{F}_{\mathrm{A}} = -kT\ln\left(\sum_{\mathrm{a}}\exp(-E_{\mathrm{a}}/kT)\right),$$

$$\tilde{F}_{\mathrm{A}} = -kT\ln\left(\sum_{\alpha}\exp(-E_{\alpha}/kT)\right).$$

Comparison of the rate constants for adiabatic and diabatic transitions shows that in any case an Arrhenius-type behaviour is realized. Especially, if only relative rates are compared one cannot distinguish between adiabatic and diabetic rate processes experimentally if only chemical homologues (regarding to the γ and w frequency behaviour) are involved.

In the case of alkali halides, where a relatively unique frequency behaviour of the molecular vibrational modes is given the relative rates of ion production $k_{\mathrm{AB}}(1)/k_{\mathrm{AB}}(2)$ of substances 1 and 2 are given as

$$\frac{k_{\mathrm{AB}}(1)}{k_{\mathrm{AB}}(2)} = \frac{\langle p_{\alpha}w_{\alpha\beta}\rangle_{(1)}}{\langle p_{\alpha}w_{\alpha\beta}\rangle_{(2)}}$$
$$\cdot \exp(F_{\mathrm{A}}(1) - \tilde{F}_{\mathrm{A}}(1) - F_{\mathrm{A}}(2) + \tilde{F}_{\mathrm{A}}(2)/kT),$$

p_{α} depending mainly on the temperature.

In all cases (adiabatic and diabatic) mentioned before the occupations of the microstates were assumed to be Boltzmann distributed. However, if the condition of energy equipartition and the assumption of a Markov process are violated, deviations from the Arrhenius type behaviour of the rate functions are expected. Such a situation could in fact occur for a fast high frequency electronic perturbation where the molecular forces would be altered with high frequency compared with the mean lattice frequencies and even thus a conservative potential description is inapplicable. In such an extreme diabatic case the transition probability is mainly determined by the overlap of the wave functions of the bound state and the system of free states of the particle:

$$w_{\mathrm{AB}} \sim |\langle \Phi_{\mathrm{bound}}|\Phi_{\mathrm{free}}\rangle|^2.$$

In this extremely diabatic approximation those transitions with maximal overlap of the wave functions are favoured. These transition probabilities have been calculated in more detail for atomic ions in [10].

In order to calculate the ratios of transition probabilities per unit time in this approximation for molecular ions (cluster ions of alkali halides) one may use the time correlation function $|C(t)|^2$ which represents the time evolution of a wave function at $t = 0$ in the bound state and the wave function at $t' = t + \Delta t$ during the interaction of the sudden perturbation:

$$\frac{w_{AB}(1)}{w_{AB}(2)} \sim \frac{|C(t)_{(1)}|^2}{|C(t)_{(2)}|^2} = \frac{|\langle \Phi(t)_{(1)} | \Phi(t')_{(1)} \rangle|^2}{|\langle \Phi(t)_{(2)} | \Phi(t')_{(2)} \rangle|^2}.$$

4. Thermodynamic Properties of Ion Formation

In part it was assumed that the ion detection threshold is mainly determined by the electron excitation process, causing comparable lattice excitation for every substance. If the irradiance is further increased for each substance by the same additional portion, again similar but higher lattice excitation should occur, in this case independant from the initiation process. For high additional irradiances it is thus possible to separate the primary excitation process from the process of ion formation.

It was shown by one of us (B. J.) that an ion formation process by gas phase reactions can be excluded (4, 11). Consequently a solid s ate evaporation model has been adopted as follows.

It is assumed that the ions are only produced directly from the crystal lattice during the laser irradiation. A solid-gas-equilibrium is not considered. No experimental evidence has been found that ion formation takes place after the laser shot. Supposing energy equipartition of all lattice degrees of freedom leading to a quasireversible isothermal ion formation process, the relative ion yields can be calculated in terms of formation enthalpy differences. The ion formation enthalpies ΔH_n for cluster ions of order n (e.g. $(Na_nCl_{n-1})^+$) were calculated by using a Born-Haber-process (see Fig. 4); thus at least the ranking of $H_n(s)$ for various alkali halide substances and ion order n is given. Thus also the ranking of the adiabatic "activation energies" $(F_C - F_A)$ are given, due to the negligible activation energy of readsorption. Although the diabatic "activation energies" $(F_0 - F_A)$ are larger with $(F_C - F_A) - (F_0 - F_A) = (F_C - F_0) = E_r$ (E_r is the relaxation energy of the sudden evaporated complex in the gasphase), the same ranking order of $(F_0 - F_A)_n(s)$ can be assumed due to analoguous bond formations of the alkali halides.

4.1. Distribution of Ion Yields and Enthalpies of Formation

The yields of cluster ions for a certain laser irradiance were determined experimentally. The mass spectra were obtained at comparable excess irradiances above threshold using a frequency doubled ruby laser ($t_p \approx 30$ ns, $\lambda = 347$ nm).

It is supposed that the experimental ion yields y_n for clusters of the order n are related to the calculated enthalpies of formation ΔH_n by

$$y_n = \frac{y_0}{n} \exp(-\Delta H_n / RT) = y_0 \exp(-\Delta G_n / RT),$$

where y_0 is the amount of substance and n^{-1} is the statistical weight of the n-cluster formed from a limited volume. y_n represents the time-integrated formation rate of the n-cluster.
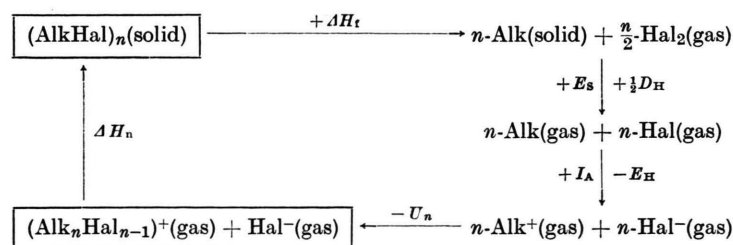

Fig. 4. Born-Haber-process used for the calculation of the formation enthalpies ΔH_n^0. ΔH_n^0 is the enthalpy of formation for clusters of the order n, ΔH_t the standard enthalpy of formation E_s the enthalpy of sublimation of the alkali metal, D_H the dissociation energy for the halogen molecule, I_A the first ionization energy of the alkali metal, E_H the electron affinity for the halogen atom, and U_n the coulomb energy difference. The data were taken from [11].
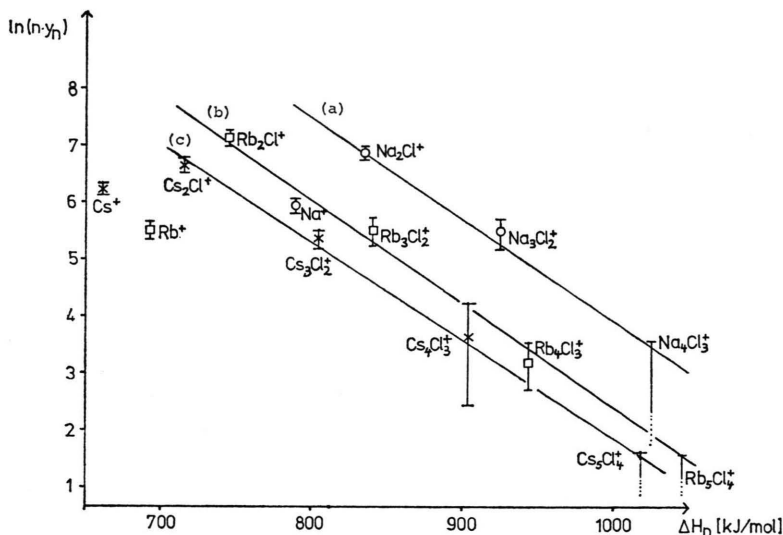
Fig. 5. Plots of $\ln(ny_n)$ vs. ΔH_n for NaCl (a), RbCl (b), and CsCl (c) using the calculated ΔH_n from the Born-Haber-process (Fig. 4) and the experimental relative yields Y_n, obtained with the same additional irradiances above the threshold energy, thus leading to nearly the same "temperatures": NaCl $T = 6300$ K, RbCl $T = 6200$ K, CsCl $T = 6700$ K.

Figures 5a—c show the normalized plots of $\ln(ny_n)$ vs. ΔH_n for CsF, CsCl and CsBr as examples. According to the model, a straight-line dependance can be fitted to the data. Similar accordance to the model is obtained for various other alkali halides. However it should be noted that in nearly all cases the salt cation occurs with lower yield than expected from this model.

The evaporation temperature due to this isothermal model may be evaluated by the slopes of the fitting lines and are typically in the range of $5000-8000$ K. In Figs. 6a—c KCl spectra are shown for three different irradiances. It was found that the temperature increases with increasing irradiance. Furthermore it can be shown from these

data that the experimental results are in contradiction to equilibrium gas phase reactions. In this case an increase in temperature would lead to a higher contribution of the entropy part in the free energy. Consequently this would lower the relative probability for the occurance of higher order clusters. Contrary to this, higher relative yields are obtained for increasing laser irradiance, in good agreement with the model of ion formation by evaporation out the solid state equilibrium.

4.2. Equimolar Mixtures under Laser Irradiation

The above simple model also provides estimates of the relative yields of cluster ions of order n (neglecting the relative heats of mixing) for mix-
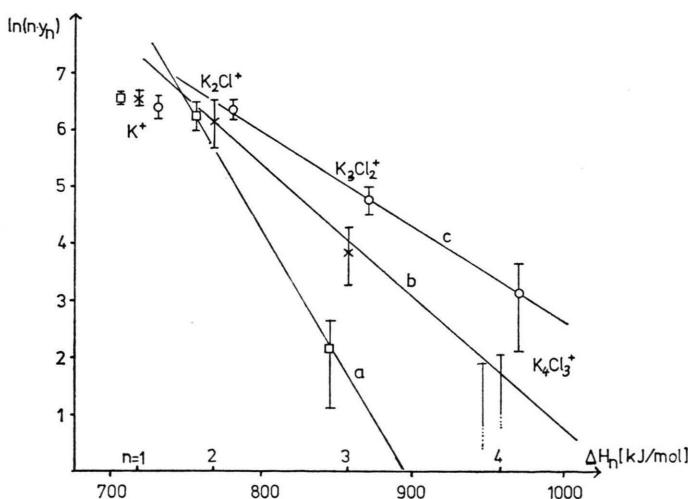

Fig. 6. Plots of $\ln(ny_n)$ vs. ΔH_n for KCl for different irradiances: a) $2E_{thr}$, b) $3E_{thr}$, c) $4E_{thr}$ (E_{thr}: threshold irradiance), leading to different "temperatures": a) $T = 2700$ K, b) $T = 4800$ K, c) $T = 6700$ K.

tures of two compounds:

$$R = \frac{y(n(1))}{y(n(2))}$$
$$= \exp(-(\Delta H(n(1)) - \Delta H(n(2))/RT).$$

For a fixed irradiance leading to a temperature of 6000 K, which is a reasonable choice due to the above cluster distributions of these salts, one expects the following yield ratios R_v for mixtures of NaCl/LiCl, NaCl/NaF, LiCl/LiF and NaF/LiF. The calculated ratios R_v are shown in Table 2 with

$$R_1 = \frac{y(Na_2Cl^+)}{y(Na_2F^+)}, \quad R_2 = \frac{y(Na_2F^+)}{y(Li_2F^+)},$$
$$R_3 = \frac{y(Na_2Cl^+)}{y(Li_2Cl^+)}, \quad R_4 = \frac{y(Li_2Cl^+)}{y(Li_2F^+)}.$$

The experimental ratios for these mixtures are also shown in Table 2. However there are experimental difficulties involved because the mixtures segregate into separate microcrystals. For this reason, the experimental values are averaged over many laser shots. Furthermore the R_v should fulfill the condition

$$R_1 R_2 = R_3 R_4.$$

This is fairly reproduced within the experimental errors.

With the typical temperature assumed above one can also calculate the ratios of charged to neutral particles when applying this model:

$$\ln(y_{n+}/y_{n0}) = (\Delta H_{n0} - \Delta H_{n+})/RT$$
for all n,

where y_{n+} are the mean yields for positively charged clusters, y_{n0} for neutral clusters of order n and ΔH_{n+} and ΔH_{n0} the corresponding enthalpies of formation. Yields of neutral clusters of order n (e.g. Alk_nHal_n) correspond to mean yields of charged clusters $(Alk_nHal_{n-1})^+$ and $(Alk_{n+1}Hal_n)^+$. These ratios for charged and neutral yields should

Table 2. Experimental and calculated (Eq. (2)) kation yield ratios R_v for equimolar mixtures.

	calc.	LID$_{exp}$	FFID$_{exp}$
R_1	8.5	3 ± 1	1
R_2	5.9	5 ± 1	5
R_3	3.5	8 ± 2	3
R_4	14.3	5 ± 2	0,3

be typically

$$y_{n0} \approx e^{11} y_{n+} \approx 10^5 y_{n+}.$$

However from ion current measurements and the quantity of the neutrally evaporated material estimated from the laser damaged volume one is able to say that

$$y_{n0} \ll 3 \cdot 10^2 y_{n+} \quad \text{in any case and}$$
$$y_{n0} \approx 20 y_{n+} \quad \text{for low irradiances}.$$

Thus the assumption of a unique quasiadiabatic process of isothermal ion and neutral formation is in severe disagreement with the experimental facts. As the ions and neutrals are formed out of the same system (the alkali halide lattice) it is thus clearly shown that the process as a whole cannot be described as a chain of quasiequilibrium states. Consequently the condition of quasiadiabaticity is ruled out. The situation is different for non-adiabatic interactions favouring ions against neutrals, which may be due to a high frequent electric coupling between the electrons and the ions.

When instead applying the method of rate processes (see Chapt. 3) for non-adiabatic transitions, one has to distinguish the cases B1 and B2. The relative rates of ion production can be roughly estimated for D in the extreme diabatic approximation. In this case yield ratios can be estimated by use of the time correlation function.

In the case of the model system (Alk Hal Alk)$^+$ the transition probability can be estimated by evaluation of the correlation time $\tau = \sqrt{J/kT}$, where J is the moment of inertia if one assumes that an amount of energy $kT/2$ is suddenly pumped into a rotatory degree of freedom. For this the correlation time is greater for greater J and consequently R_v can be estimated as

$$\frac{y_I}{y_{II}} \approx \sqrt{\frac{J_I}{J_{II}}} \quad \text{and} \quad \begin{array}{ll} R_1 \approx 1.3, & R_2 \approx 2.1, \\ R_3 \approx 2.0, & R_4 \approx 1.3. \end{array}$$

Comparison of the above calculated R_v with the experimental ones also shows a good agreement within the errors.

4.3. Equimolar Mixtures under Fission Fragment Induced Desorption

The experimental results for equimolar mixtures ^{252}Cf-fission fragment induced desorption (ffid) are also given in Table 2. In the case of ffid, ion forma-

tion cannot be explained by an adiabatic process. When assuming a purely thermal evaporation one can calculate the evaporation rate from the statistic gas theory:

$$\frac{dn}{dt} = \frac{F\,p(T)}{(2\pi\,MRT)^{1/2}} \,,$$

where $p(T)$ is the vapour pressure, F the excited area, M the mass of the produced particles, and the evaporation and recombination rates are provided to be equal. Typical ion formation times are in the range of at most 100 ps and the excited area is about some 10^{-17} m^2 (the screening length of an electric excitation in the medium).

Thus for ffid the above equation yields about 1 particle per 100 ps and from the ratio of ion to neutral yield calculated before, the ion yield is lower than 10^{-4} ions/100 ps for any assumed temperature. Experimentally an ion yield of about $1-5$ ions per fission fragment is obtained, in sharp contrast to the above adiabatic assumption.

However, also rate calculations for a diabatic process may fail because in this case one is not able to start from the assumption of energy equipartition of the surrounding condensed medium (the excitation times are within $10^{-14}-10^{-15}$ s) or from the equilibrium distribution of the microstates in the bound electronic state. In this case deviations from the Arrhenius-type behaviour of the diabatic ion production kinetics may occur, although the order of magnitude is at least represented. With the excited area given above some tens of molecules are affected at the surface with a reasonable $p_\alpha w_{\alpha\beta} \sim 10^{12}$ s^{-1} for alkali halide clusters and within the interaction time 10^{-12} s several ions are expected to be produced. It is interesting to note that the rates of ion formation under laser irradiation are also larger than expected from statistic gas theory with the temperatures calculated in Chapter 4.1.

When nevertheless comparing the experimental ratios for ffid in Table 2 with those calculated in the extreme diabatic approximation one will find that these R_v are a much better approximation one will find that these R_v are a much better approximation to the experiment than those calculated from the adiabatic model presented before.

5. Source Depth of Ion Formation

The model presented in 4.1 in analogy to 4.2 for mixtures of two alkali halides (with concentrations

c_1 and c_2) predicts a yield ratio

$$R = \frac{y_n(1)}{y_n(2)} = \frac{c_1}{c_2} \cdot \exp\left(-\left(\Delta H_n(1) - \Delta H_n(2)\right)/RT\right).$$

Different mixtures of two compounds with a concentration ratio $c_1/c_2 = 1000$ were investigated. The experimental and calculated data for these mixtures are shown in Table 3. It can be seen from the table that the calculated ratios are only represented experimentally for those mixtures where the ionic radii of the adduct ions are smaller than those of the matrice ions whereas large deviations occur in the opposite case.

The hypothesis that the adduct ions are stochastically distributed in the lattice of the matrix substance can be ruled out for adducts with the larger ionic radius. Differences of the band gaps as well as formation enthalpy differences between the two compounds would be assimilated and thus no preference of ions of the one compound could occur. For adducts with minor ionic radii this hypothesis does not lead to contradictions with the experimental results.

For larger ionic radii of the adducts one can assume that interface phenomena are dominant (segregation of the adduct material from the matrix compound). This and the assumption that the above equation is also able to describe these phenomena leads to two different possibilities:

a) lower formation enthalpies of the interface-phase substances ($\delta\Delta H \cong 2.5-3.5$ eV),

b) higher electronic absorption of the interface-phase material due to lower order structure, leading to a higher excitation temperature.

Table 3. Kation yield ratios of the adducts obtained experimentally by LID at an irradiance of about $3\,E_{\text{thr}}$, and calculated yield ratios from Eq. (3) for $T = 6000$ K. The molar concentration of the matrix substance c_1 was in all cases 10^3 times that of the adduct substance c_2.

matrix substance	adduct substance	$\left(\dfrac{y_1(1)}{y_1(2)}\right)_{\text{exp}}$	$\left(\dfrac{y_1(1)}{y_1(2)}\right)_{\text{calc}}$
NaCl	LiCl	~ 100	3900
NaCl	KCl	1.2	230
NaCl	RbCl	1.6	140
NaCl	CsCl	1.0	70
RbCl	LiCl	~ 100	28500
RbCl	NaCl	~ 100	7200
RbCl	KCl	~ 100	1650
RbCl	CsCl	2.0	530

The decrease of the relative ion yields of the interface material with increasing laser irradiance provides a ratio of the probabilities of excitation of interface and matrix material under any of the above assumptions.

Under the specific assumption a) and from the ratio of neutral to charged evaporated material (see 4.2) one can calculate the maximum number m of atomic layers being evaporated from the interface.

For the calculation of an upper limit of m the following extreme assumption is made:

The adduct component as a part only of the interphase component is evaporated completely as charged particles (degree of ionization $= 1$) whereas the matrix component is evaporated with a neutral to charged ratio of $y_{n0}/y_{n+} \ll 300$. From this and the R in the table follows that the number m of atomic layers of the interface phase (regarding to the ion formation out of the different components) is

$$m < \frac{y_{n0}(\mathrm{Na})}{y_{n+}(\mathrm{Na})} \cdot \left(\frac{y(\mathrm{Na})}{y(\mathrm{K})} \right)_{\mathrm{exp}} = 300 \,,$$

where $(y(\mathrm{Na})/y(\mathrm{K}))_{\mathrm{exp}}$ is the experimentally obtained yield ratio for $c(\mathrm{Na})/c(\mathrm{K}) = 1000$. Thus realistic values of m may be in the order of ten for the above irradiation conditions.

From § 5. follows that laser induced ion formation from alkali halides can neither be regarded as a pure monolayer surface phenomenon nor as a pure bulk evaporation, but is found to be a nonequilibrium surface phase transition! Thus the thermodynamic properties of § 4. being bulk values can hardly be considered as absolute values governing the ion formation process. However, the relative values are not affected by this restriction.

By the way, similar adduct effects are often observed with polar organic compounds [12].

[1] N. Fürstenau and F. Hillenkamp, Int. J. Mass Spectr. Ion Phys. **37**, 135 (1981).
[2] N. Fürstenau, Symposium: Ion Formation from Organic Solids (Münster 1980) Springer Tracts in Chemical Phys. in press.
[3] F. R. Krueger and B. Schueler, Adv. Mass Spectrom. **8**, 918 (1980).
[4] B. Jöst, Diploma Thesis, Frankfurt 1981.
[5] N. Fürstenau, Doctoral Thesis, Frankfurt 1981.
[6] W. Ludwig, Festkörperphysik, Uni-text, Heidelberg 1981.
[7] A. Schmid, P. Kelly, and P. Bräunlich, Phys. Rev. **B 16**, 4569 (1977).
[8] B. Fain, Physica **101 A**, 67 (1980).
[9] B. Fain, Theory of Rate Processes in Condensed Media, Lecture Notes in Chemistry (Springer, New York 1980.)
[10] F. R. Krueger, Surface Sci. **86**, 246 (1979).
[11] M. F. Ladd, Structure and Bonding in Solid State Chemistry, John Wiley, Chichester 1979.
[12] B. Schueler, P. Feigl, F. R. Krueger, and F. Hillenkamp, Org. Mass Spectrom. **16**, 502 (1981).
[13] B. Schueler, R. Nitsche, and F. Hillenkamp, Proc. of the Scanning Electron Microscopy Conf., O'Hare, USA, 1980.